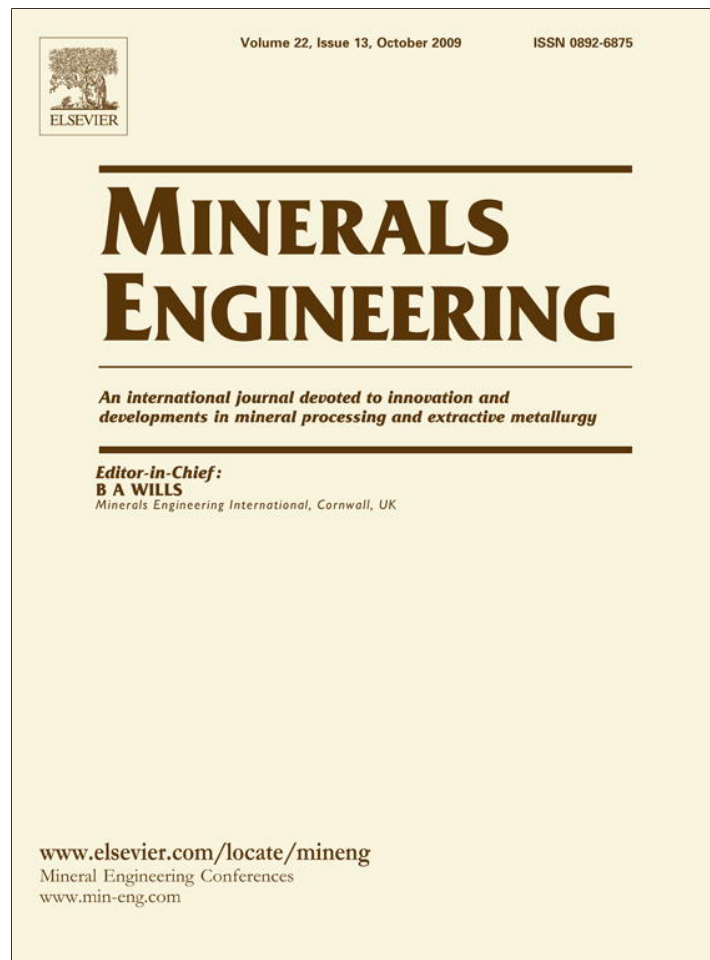


Provided for non-commercial research and education use.
Not for reproduction, distribution or commercial use.



This article appeared in a journal published by Elsevier. The attached copy is furnished to the author for internal non-commercial research and education use, including for instruction at the authors institution and sharing with colleagues.

Other uses, including reproduction and distribution, or selling or licensing copies, or posting to personal, institutional or third party websites are prohibited.

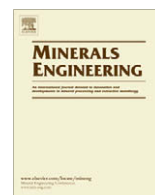
In most cases authors are permitted to post their version of the article (e.g. in Word or Tex form) to their personal website or institutional repository. Authors requiring further information regarding Elsevier's archiving and manuscript policies are encouraged to visit:

<http://www.elsevier.com/copyright>



Contents lists available at ScienceDirect

Minerals Engineering

journal homepage: www.elsevier.com/locate/mineng

A novel approach for the modelling of high-pressure grinding rolls

M. Torres, A. Casali*

Mining Engineering Department, University of Chile, Chile

ARTICLE INFO

Article history:

Received 3 December 2008

Accepted 28 April 2009

Available online 22 May 2009

Keywords:

Modelling

Grinding

Sulphide ores

ABSTRACT

The HPGR technology has become more attractive to the copper industry because of its high throughput capacities and its low specific energy consumptions. A HPGR model, able to give enough information based on pilot plant testing, in order to back up HPGR engineering studies, was developed. The model was based on the physical phenomena of the grinding operation. The model parameters were fitted with pilot scale test results, corresponding to a Chilean copper ore, classified in two lithologies (andesitic and porphyritic ores). Some sets of data were not used in the fitting stage, to test the predictive capability of the model. The pilot scale tests were performed at the facilities of two HPGR manufacturers, changing operating pressure and rolls peripheral velocity (only one of the manufacturers). The simulated specific energy consumptions and particle size distributions, compared with the experimental data, were considered good enough. The model was able to predict adequately throughput capacity, specific energy consumption and particle size distributions of the edge, centre and total products.

© 2009 Elsevier Ltd. All rights reserved.

1. Introduction

High-pressure grinding rolls (HPGR) technology has struggled for acceptance into the hard-rock mining sector, has had many advances in this sector, but is still regarded as an “immature” technology (Bearman, 2006). It has been applied to progressively harder, tougher and more abrasive materials, generally successfully, but not without some problems (Morley, 2006).

The HPGR consists of two counter-rotating rolls mounted in heavy-duty frictionless bearings, enclosed in a strong frame. Pressure is applied to one of the rolls that can move linearly by means of a hydro-pneumatic spring system, while the other roll is held in a fixed position in the frame (Klymowsky et al., 2002). The pressure exerted by the hydraulic system on the floating roll, that allows horizontal movement of the moving roll, largely determines comminution performance. Typically, operating pressures are in the range of 5–10 MPa, but can be as high as 18 MPa. For the largest machines, this translates to forces of up to 25,000 kN (Morley, 2006). The rolls are driven by separate motors and can be operated at fixed or variable speed (Klymowsky et al., 2002). In most mineral applications, the roll surfaces are protected by implanting tungsten carbide studs that help to form an autogenous wear layer on the rolls and improve the drawing of the material into the rolls (Klymowsky et al., 2002).

Roll diameters of industrial and semi-industrial units vary from 0.8 to 2.8 m. Capacities range from 50 to up to 3000 t/h. Energy consumption is between 1 and 3 kWh/t (Klymowsky et al., 2002).

There are currently three recognized manufactured of HPGR machines, namely Polysius, KHD Humboldt Wedag and Köppern, all based in Germany (Morley, 2006).

At present, the three HPGR producers will all give guarantees of throughput and useful life of their equipment, as long as they complete sufficient representative test work (Danilkewich and Hunter, 2006). The test work will require obtaining ore representative samples and sending around 1000–1500 kg samples to the manufacturers and they will run HPGR amenability tests. After this phase is completed, pilot or semi-industrial testing with additional samples will be required. HPGR suppliers stipulate that scale-up of pilot units should be done with caution. The main objectives of material testing are to determine: the ore suitability to HPGR grinding, the parameters required for sizing (specific throughput and specific grinding force), the achievable product size distribution and the abrasiveness of the ore (Klymowsky et al., 2002). In terms of energy consumption, the traditional Bond theory to estimate the energy requirements can not be used because it grossly underestimates the actual grinding energy of the HPGR (van Dru-nick and Smit, 2006).

Several tests have been developed in order to quantify the behaviour of different ores in the various crushing and grinding applications (Bond work index, JK Drop weight test, SAG power index, etc.). However, none of these tests can be applied to high-pressure grinding (Patzelt et al., 2006). Accordingly, the only remaining alternative is the use of pilot or semi-industrial testing data. The properties of an ore have a far greater impact on achievable fines production than the grinding force (Patzelt et al., 2006). The product fineness is controlled by the grinding force applied to the material bed between the rolls, causing micro-cracks and breakage of

* Corresponding author. Tel.: +56 2 9784477.

E-mail address: dirdimin@ing.uchile.cl (A. Casali).

the particles. The correlation between particle breakage and the grinding force required needs to be determined for each material.

At present, in a greenfield hard-rock application, to include HPGR in a flow sheet relies on its ability to provide a significant reduction in comminution costs at a similar operating availability (Danilkevich and Hunter, 2006). Testing methods and quantity of sample to be tested is yet to be defined. New methods and approaches are being developed, but some gaps exist and in particular the requirements for ore body variability testing. Circuit design issues also remain to be a point of discussion (Danilkevich and Hunter, 2006).

Successful pilot-plant testing carried out in the last years has proven the operational reliability of HPGR technology in hard rock applications. As an important result for the copper industry six HPGRs were commissioned in two copper concentrators in 2006, four in South America and two in Indonesia (Patzelt et al., 2006). In both cases, the producers' decision was based on the energy savings and low operating costs of the HPGRs, compared with those obtained with alternative technologies.

A relevant case is the conceptual engineering study for the Los Bronces expansion project (Oestreicher and Spollen, 2006). In this study a HPGR circuit and a SAG circuit were designed and compared for an 80,000 t/d expansion. This operation is located in Chile and it is among the largest copper resources in the world. As in this case at least in other three Chilean mining operations or projects the HPGR technology is under consideration and pilot-plant testing has been carried out or will be performed in the near future.

With respect to modelling of the high-pressure grinding roll, the most important work was done by Morrell and some co-authors (Morrell et al., 1997; Daniel and Morrell, 2004). The Morrell et al. model consists of three parts: a model for the prediction of product size distribution, a throughput model and a power consumption component. The throughput model uses a standard plug flow model. The power consumption is based on the throughput and the specific grinding energy, E . To model the product size distribution three separately defined processes (assumed as independent breakage mechanisms) are modelled and then combined.

In the pre-crusher zone, if particle are bigger than a certain critical size, they will be broken directly by the roll faces as would occur in a conventional roll crusher. For Klymowsky et al. (2002) the largest particle nipped between the rolls in the compression zone would be about 1.5 times the gap. Larger particles would cause the separation of the rolls and the collapse of the compression zone, with the resulting reduction in grinding efficiency.

The Morrell et al. model considers that breakage at the edge of the rolls is different to that at the centre and is more similar to that occurring in a conventional roll crusher (Daniel and Morrell, 2004). This edge effect explains the proportion of relatively coarse particles seen in HPGR products. No compressed bed breakage is assumed to take place in this zone. The interface between the compression zone and the edge effect zone is represented by a fraction of the original feed material which undergoes single particle comminution.

Since the HPGR technology is based on applying high pressures, the compression zone is by far the most important comminution zone, as it is where the majority of the breakage processes take place. Under normal HPGR process conditions the edge and pre-crusher parts of the model are not dominant, but contribute to the overall accuracy (Daniel and Morrell, 2004).

Several aspects of this model, regarding the prediction of product size distribution, are not well explained or are not detailed. For example, with respect to some parameters as the ore specific split factor or the correction factor used in the equation to predict throughput, are they fitting parameters? Must be determined experimentally? With respect to the compression zone, what is the model describing the breakage in this zone? How is included

the rolls speed, which has an effect (Lim et al., 1997) on the shape of the product size distributions, particularly at the coarser sizes, producing a steeper size distribution? The rolls speed is included in the throughput predictor, as well as indirectly in the power draw predictor, but it should also be considered for the prediction of the product size distribution. The predictions of this model were considered good for the authors, but also strongly dependent of the characteristics of the material being tested and is said to be ore specific (Daniel and Morrell, 2004).

The main goal of this work is to model the HPGR operation, for the development of a simulator able to give enough information, based on pilot plant testing, in order to back up the continuation to more advanced steps in potential HPGR engineering studies. The HPGR model will be fitted with pilot data, corresponding to a Chilean copper ore. Some sets of data will be kept apart and will not be used in the fitting stage, to test the predictive capability of the model.

2. Modelling

The high-pressure grinding rolls model presented in this paper is a set of equations that on the basis of the ore characteristics, equipment dimensions and operating conditions is able to predict the equipment performance in terms of throughput, power consumption and particle size distribution of the product.

The model structure has its basis on the work developed by Morrell et al. at the JKMRRC. Both models, the proposed by Morrell et al. (Daniel and Morrell, 2004) and the one presented here, include the pre crusher effect for certain particle sizes, nevertheless a novel approach for the prediction of the different particle sizes along the roll axis (edge and centre) is presented.

The model equations are based on physical phenomena that govern the operation: mass balances for throughput estimation, physics equations for the power consumption and a population balance model for the particle size distribution.

The stream of particles inside the comminution zones in the HPGR is limited by the roll surfaces and the liner patterns, and it is modelled as a plug flow. This hypothesis has been accepted by researchers and manufacturers (Daniel and Morrell, 2004).

The plug flow hypothesis is the base of the modelling; the applying of this criterion in the deduction of the model equations is discussed next.

As it has been discussed, the HPGR model is made up of three sub-models which predict the throughput, power draw and the particle size distribution. Fig. 1 shows a general schema of the HPGR, which had been used to develop the mathematical expressions of the model.

2.1. Throughput model

The theoretical tonnage treated by a HPGR of diameter D (m), length L (m) and operating gap s_0 (m), is calculated from a steady-state mass balance of the ore flowing in the particle bed compression zone. In Fig. 1, the centre of mass of a band of ore with width $s(\alpha)$ is defined by the position vector $r(\alpha)$. The motion equation is described as a function of the angle α as follows:

$$r(\alpha) = \frac{1}{2}(D + s_0)\hat{i} + \frac{D}{2} \sin \alpha \hat{k} \quad (1)$$

Thus, the velocity of the band, $v(\alpha)$, is calculated by the first derivative of the position vector shown in Eq. (1). Considering that the rolls angular velocity is constant and equal to $2U/D$, being U the peripheral velocity (m/s), the resulting velocity of the band is shown in Eq. (2) as follows:

$$v(\alpha) = \frac{D}{2} \frac{2U}{D} \cos \alpha \hat{k} = U \cos \alpha \hat{k} \quad (2)$$

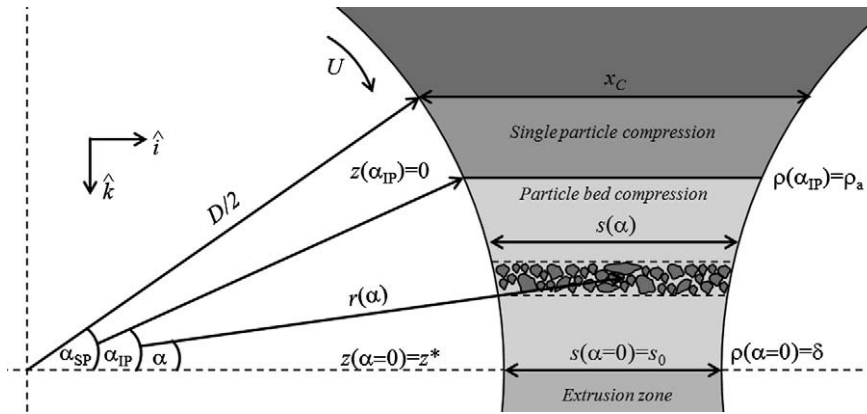


Fig. 1. Conceptual schema of the HPGR.

The density of the ore band at any angle α is $\rho(\alpha)$. At the beginning of the particle bed compression zone (defined by the angle $\alpha = \alpha_{IP}$), $\rho(\alpha)$ is equivalent to the feed bulk density, ρ_a . Also, be δ the ore band density at the extrusion zone ($\alpha = 0$).

The tonnage of the ore band, G_S (t/h), with $\rho(\alpha)$ expressed in t/m^3 , is written as a function of the angle α in Eq. (3).

$$G_S(\alpha) = 3600\rho(\alpha)s(\alpha)LU \cos \alpha \quad (3)$$

The width of the ore band as a function of the angle α can be expressed as:

$$s(\alpha) = s_0 + D(1 - \cos \alpha) \quad (4)$$

Under steady state conditions the difference of tonnage between the beginning and the end of the particle bed compression zone is equal to zero. Using Eqs. (3) and (4), with the corresponding α values and considering that $\rho(\alpha_{IP}) = \rho_a$ and $\rho(\alpha = 0) = \delta$, the following quadratic equation, whose unknown values are the cosines of the inter particle compression angle, is obtained:

$$\rho_a D \cos^2 \alpha_{IP} - \rho_a (s_0 + D) \cos \alpha_{IP} + \delta s_0 = 0 \quad (5)$$

Only the higher root is considered in the solution, because it is the only one to give acceptable values for the α_{IP} angle (the smaller root gives smaller cosines and too higher angles). The solution is shown in Eq. (6).

$$\cos \alpha_{IP} = \frac{1}{2D} \left[(s_0 + D) + \sqrt{(s_0 + D)^2 - \frac{4s_0\delta D}{\rho_a}} \right] \quad (6)$$

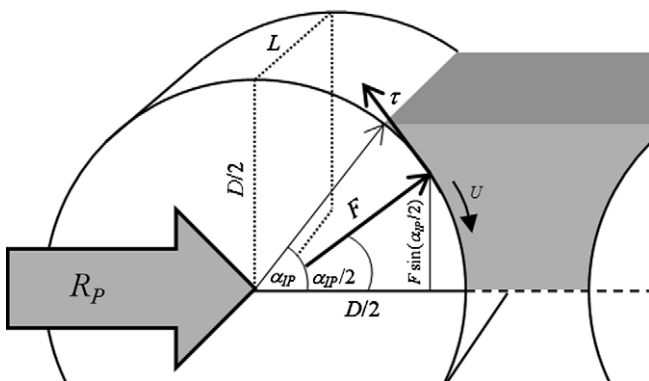


Fig. 2. Simplified force diagram in a HPGR of roll width D and length L . The operating pressure R_p , the compression force, F , its vertical component and the resulting torque, τ , are shown. The dotted lines inside the roll represent the projected area where the operating pressure is exerted.

Thus, the throughput can be calculated with Eq. (3) at any of the borders. In particular at the extrusion zone ($\alpha = 0$), the throughput can be calculated as:

$$G_S = 3600\delta s_0 LU \quad (7)$$

2.2. Power draw model

Fig. 2 shows a forces diagram in the HPGR. The force applied to the material at the particle bed compression zone is called the Compression Force, F (kN), which is calculated using the rolls operating pressure, R_p (bar), multiplied by the projected area where it is applied, as it is shown in Eq. (8). Since the HPGR is operated in a choke fed condition, the applied pressure is distributed only in the upper right half of the roll (as it is shown in Fig. 2). Then the projected area considered should be $\frac{D}{2}L$.

$$F = 100R_p \frac{D}{2}L \quad (8)$$

Eq. (8) is similar in structure as the one proposed by Austin (1997) for the calculation of the grinding pressure, but was obtained by a direct relation.

Klymowsky et al. (2006) recommends a value for the angle of action of this force as half the inter particle compression angle α_{IP} . The vertical component of this force exerts a torque τ (kN m) in each roll, which can be written (see Fig. 2) as:

$$\tau = F \sin \left(\frac{\alpha_{IP}}{2} \right) \frac{D}{2} \quad (9)$$

As the power required to spin both rolls is equal to twice the torque multiplied by the rolls angular velocity, then the total power draw P (kW) can be expressed as:

$$P = 2F \sin \left(\frac{\alpha_{IP}}{2} \right) U \quad (10)$$

The specific energy consumption W (kWh/t) is expressed as the ratio between the power draw (kW) and the throughput (t/h), as follows:

$$W = \frac{P}{G_S} \quad (11)$$

2.3. Particle size distribution model

The HPGR is considered as a series of two size reduction stages. The differences between the stages are the breakage mechanisms. Fig. 3 shows the structure for the particle size distribution model.

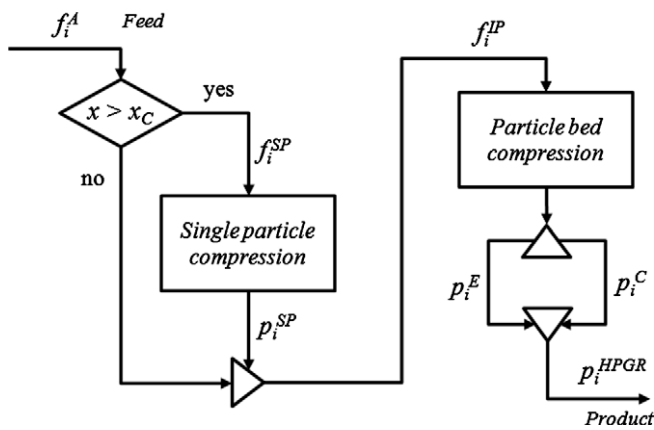


Fig. 3. Particle size distribution model schema.

In the single particle compression zone, located between the angles α_{SP} and α_{IP} (see Fig. 1), particles larger than a certain size x_C are broken instantly due to compression by the rolls (Daniel and Morrell, 2004). The critical size x_C is obtained by replacing the inter particle compression angle α_{IP} in Eq. (4), as follows:

$$x_C = s(\alpha_{IP}) = s_0 + D(1 - \cos \alpha_{IP}) \quad (12)$$

The product size distribution of the single particle compression zone, p_i^{SP} , can be written, assuming that every particle will break instantaneously at the same rate, as follows:

$$p_i^{SP} = \sum_{l=1}^N b_{il} f_l^{SP} \quad (13)$$

where b_{il} is the fraction of particles of size “l”, which by comminution is reduced to size “i”; f_l^{SP} is the fraction in size class “l” of the mineral going to the single particle compression stage (class of size $x > x_C$).

The product of the single particle compression zone rejoins with the fraction of material of size lesser or equal than the critical size x_C , forming beds of particles with a particle size distribution, f_i^{IP} , which feed the inter particle compression zone. According to several authors (Klymowsky et al., 2002; Daniel and Morrell, 2004; Patzelt et al., 2006) the particle bed compression zone produces two different particle size distributions, at the edge (more coarse), p_i^E , and at the centre of the rolls, p_i^C . Lubjuhn (1992) explained this phenomenon when he found that the pressure profile exerted over the rolls is similar to a parabola, as it is shown in Fig. 4. Following this approach, the roll where the pressure is applied was discret-

ized on N_B blocks. In each one, a different compression force depending on the pressure profile is applied. Accordingly, each one of these blocks will have a particular power consumption and a particular rate of breakage. Obviously, the product will be coarser on the edge of rolls due to lower rates of breakage.

On each block, the material is broken gradually as it reaches the extrusion zone. The intensive property $m_{i,k}$ (mass fraction retained by weight in size class i, in each block k) is a function of the vertical position, z (see Fig. 1), so a microscopic population balance model is applied for each of the N size classes. The model required is a steady state model. A plug flow condition is assumed as well as a constant velocity in the z direction, v_z .

Under these considerations, the model equation consists in a system of $N \times N_B$ differential equations, each one for the size class i ($i = 1, \dots, N$) in each block k ($k = 1, \dots, N_B$; see Fig. 4), as the one shown in Eq. (14).

$$v_z \frac{d}{dz} m_{i,k}(z) = \sum_{j=1}^{i-1} S_{j,k} b_{ij} m_{j,k}(z) - S_{i,k} m_{i,k}(z) \quad (14)$$

where $S_{i,k}$ is the rate of breakage of particles of size i in each block k; b_{ij} is the fraction of particles of size “j”, that by comminution is reduced to size “i”. It is considered independent of the block and is assumed that it has the same value than the corresponding to the single particle compression zone.

To solve these equations the following border conditions are used:

$$m_{i,k}(z = 0) = f_i^{IP} \text{ and } m_{i,k}(z = z^*) = p_{i,k}$$

where $p_{i,k}$ is the mass fraction retained by weight in size class i, in the product of each block k, z^* is the vertical distance from the entrance to the particle bed compression zone to the extrusion zone, which can be calculated geometrically (see Fig. 1) as follows,

$$z^* = \frac{D}{2} \sin(\alpha_{IP}) \quad (15)$$

Eq. (14) is similar to the batch grinding kinetic equation, which has been solved analytically (Reid, 1965). The system solution for the N size classes and the N_B blocks is written as follows,

$$p_{i,k} = \sum_{j=1}^i A_{ij,k} \exp\left(-\frac{S_{j,k}}{v_z} z^*\right) \quad (16)$$

where

$$A_{ij,k} = \begin{cases} 0 & i < j \\ \sum_{l=j}^{i-1} \frac{b_{il} S_{l,k}}{S_{i,k} - S_{j,k}} A_{lj,k} & i > j \\ f_i^{IP} - \sum_{l=1}^{i-1} A_{il,k} & i = j \end{cases} \quad (17)$$

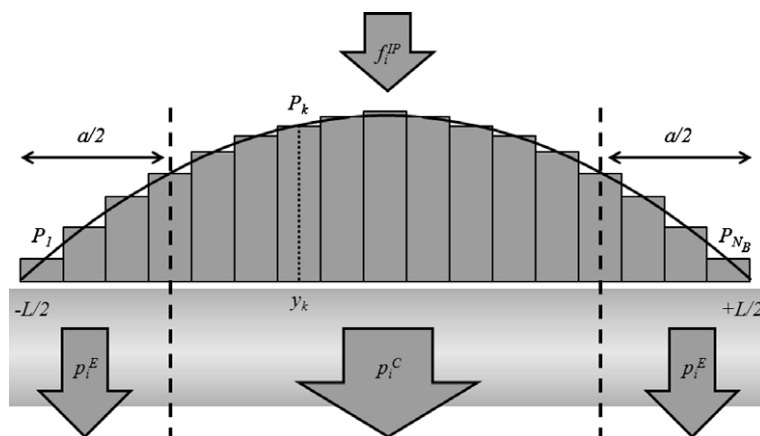


Fig. 4. Discretization of the roll, its pressure profile and the resulting edge and centre particle size distributions.

For the breakage functions, b_{ij} , the functional expression (Austin and Luckie, 1972) presented in Eq. (18) will be used.

$$B_i(x_i) = \alpha_1 \left(\frac{x_i}{x_2}\right)^{\alpha_2} + (1 - \alpha_1) \left(\frac{x_i}{x_2}\right)^{\alpha_3} \quad (18)$$

where α_1 , α_2 and α_3 are model parameters to be adjusted with the experimental data. B_i is the cumulative form of the b_{ij} functions, determined as follows,

$$b_{ij} = \begin{cases} B_{i-j+1} - B_{i-j+2} & i > j \\ 1 - \sum_j b_{ij} & i = n \\ 0 & i \leq j \end{cases} \quad (19)$$

For the breakage rate, the functional expression (Herbst and Fuerstenau, 1980) presented in Eq. (20) is used. The advantage of using this expression lies on the scale up relationship among the specific rate of breakage, S_i^E , invariant, and the quotient between Power, P_k and Holdup, H_k , which will vary depending on the block k considered, as it is shown in Eq. (21).

$$\ln(S_i^E/S_1^E) = \zeta_1 \ln(\bar{x}_i/\bar{x}_1) + \zeta_2 \ln(\bar{x}_i/\bar{x}_1)^2 \quad (20)$$

$$S_{i,k} = \frac{P_k}{H_k} S_i^E \quad (21)$$

where ζ_1 , ζ_2 and S_i^E are model parameters to be adjusted with the experimental data.

The Holdup of each block k , at the particle bed compression zone, is calculated as follows,

$$H_k = \frac{1}{N_B} G_S \frac{z^*}{3600U} \quad (22)$$

As was above mentioned (Lubjuhn, 1992) the pressure profile exerted over the rolls may be represented by a parabola. Accordingly, the power consumption by each block, P_k , can be calculated using Eq. (10) as it is shown in Eq. (23),

$$P_k = 2F \sin\left(\frac{\alpha_{IP}}{2}\right) U \frac{(L^2 - 4y_k^2)}{\sum_{j=1}^{N_B} (L^2 - 4y_j^2)} \quad (23)$$

where y_k corresponds to the position of the centre of block k (see Fig. 4), which is calculated as follows,

$$y_k = \frac{L}{2N_B} (2k - N_B - 1) \quad (24)$$

Be a the fraction of ore produced in the edges of the rolls. The number of blocks E considered to calculate the particle size distribution of the edge product is equal to $0.5 a N_B$.

In mathematics the floor function, $[E]$, is defined as the largest integer less than or equal to E . Also the ceiling function, $\lceil E \rceil$, is defined as the smallest integer not less than E . With these definitions, the particle size distribution of the edges product, p_i^E (see Fig. 3), is calculated as:

$$p_i^E = \frac{1}{E} \left[\sum_{k=1}^{\lceil E \rceil} p_{i,k} + (E - \lceil E \rceil) p_{i, \lceil E \rceil} \right] \quad (25)$$

The particle size distribution of the total product, p_i^{HPGR} (see Fig. 3), can be calculated as the joint distribution of the edge, p_i^E , and centre, p_i^C , zones (Eq. (27)) or as the average of all the blocks, as it is shown in Eq. (26).

$$p_i^{\text{HPGR}} = \frac{1}{N_B} \sum_{k=1}^{N_B} p_{i,k} \quad (26)$$

The particle size distribution of the centre product then, is calculated by balance using Eq. (27) as follows,

$$p_i^C = \frac{1}{1-a} (p_i^{\text{HPGR}} - a p_i^E) \quad (27)$$

A working example, showing the step-by-step calculation results for one prediction, is presented in Appendix A.

3. Experimental data

To test the potential use of HPGR technology in the feasibility studies for a new project, an important Chilean copper producer decided to send several samples of two lithologies present in their ore to two HPGR manufacturers. These samples were treated in pilot units changing different operating conditions.

The deposit is located in northern Chile and its ore is classified in two main geological units: Porphyric and Andesitic copper ore. To match the feed requirements for the equipment, the samples were crushed and screened to an approximate top size of 40 mm. Sub-samples of 150 kg were taken by coning and quartering for ore characterisation and to perform the tests on the pilot scale HPGR.

The grinding tests consisted in a series of open and locked circuit tests to measure the specific energy consumption, W , and the particle size distribution of the product as a function of variables such as the roll operating pressure and peripheral velocity. For model validation purposes, only the open circuit tests will be considered in this work.

The specific gravity of both andesitic and porphyric ore were measured by the first manufacturer, being 2.74 for the porphyric ore and 2.80 for the andesitic ore.

The pilot HPGR used by the first manufacturer, M1, has studded rolls of 800 mm of diameter and 250 mm of length. In the tests, the rolls peripheral velocity, U , and the operating pressure, R_p , are operating variables. The results of the open circuit tests done by this manufacturer are shown in Tables 1 and 2.

The pilot HPGR used by the second manufacturer, M2, also has studded rolls, but of 710 mm of diameter and 210 mm of length. In the tests, the rolls peripheral velocity, U , was constant at 0.29 m/s while the operating pressure R_p , was variable between 30 and 50 bar. The results of the tests done by the second manufacturer are shown in Tables 3 and 4.

Selected results, corresponding to manufacturer M1, are shown in Fig. 5. These results show that for different operating pressures, R_p , different product size distributions are obtained, as can be observed from the comparison of M1-P1 vs. M1-P6 and M1-A1 vs. M1-A5 (same ore, different R_p). It is also evident that if the ore is different but the operating pressure is the same, different product size distributions are obtained. However, the effect is very small, especially with a higher R_p , as can be observed from the comparison of M1-P6 vs. M1-A5. With a lower R_p the differences are more evident (M1-P1 vs. M1-A1). In the case of manufacturer M2, almost the same situation is observed, with a small effect of the operating pressure (lower R_p were used) and also a very small effect caused by the different ore treated.

4. Model fitting and validation

As was explained in chapter 2, the HPGR model developed in this work, consists in a throughput equation (Eq. (7)) and a power draw equation (Eq. (10)), combined in a specific energy consumption equation (Eq. (11)); and a particle size distribution model (Eqs. (16), (25), (26), and (27)). The prediction quality of the specific energy consumption model is shown in Fig. 6. All data values were used in the validation because the specific energy consumption model is general and do not consider specific parameters for each manufacturer-ore type combination.

The correlation coefficient for the modelled and experimental values is 80%. As can be seen in Fig. 6, a single experimental data

Table 1
Summary of open circuit tests results performed by manufacturer M1 with porphyritic copper ore.

Test	Feed	M1-P1	M1-P2	M1-P3	M1-P4	M1-P5	M1-P6	M1-P7
<i>Operating conditions</i>								
<i>U</i> (m/s)		0.67	0.37	0.67	0.97	0.67	0.66	0.66
<i>R_p</i> (bar)		41	61	61	60	76	76	61
Size (mm)	Percent passing (%)							
45.00	100.00	100.00	100.00	100.00	100.00	100.00	100.00	100.00
31.50	97.61	100.00	100.00	100.00	100.00	100.00	100.00	100.00
22.40	57.60	98.36	98.92	99.71	99.33	100.00	100.00	100.00
16.00	36.71	84.87	96.46	92.52	92.16	94.93	96.39	94.77
11.20	25.81	71.80	88.77	83.85	83.25	84.84	89.17	84.90
8.00	20.32	61.82	78.95	74.73	72.00	75.54	81.10	74.94
5.60	15.91	52.82	68.91	65.18	62.67	66.75	70.48	65.41
2.80	10.49	39.19	54.60	49.91	47.88	51.86	55.53	49.84
1.00	6.75	25.25	36.39	32.66	31.54	34.93	38.01	33.20
0.50	5.16	19.49	28.67	25.27	24.76	27.70	30.23	25.97
0.32	4.31	16.69	24.95	22.26	21.49	24.19	26.42	22.42
0.20	3.43	14.06	21.43	19.13	18.41	20.83	22.76	19.36
0.13	2.58	11.75	18.34	16.42	15.72	17.80	19.56	16.09
<i>Specific power consumption</i>								
<i>W</i> (kWh/t)		1.44	2.06	2.03	2.04	2.40	2.48	1.98

Table 2
Summary of open circuit tests results performed by manufacturer M1 with andesitic copper ore.

Test	Feed	M1-A1	M1-A2	M1-A3	M1-A4	M1-A5	M1-A6
<i>Operating conditions</i>							
<i>U</i> (m/s)		0.67	0.37	0.67	0.97	0.66	0.66
<i>R_p</i> (bar)		39	60	60	60	75	59
Size (mm)	Percent passing (%)						
31.50	96.32	100.00	100.00	100.00	100.00	100.00	100.00
22.40	65.50	100.00	100.00	100.00	100.00	100.00	99.63
16.00	43.26	94.19	96.52	96.85	97.19	96.34	96.54
11.20	30.93	83.39	85.73	87.29	87.91	88.31	86.44
8.00	22.68	70.62	74.98	75.12	76.31	77.78	76.09
5.60	17.47	59.25	64.67	64.77	65.45	67.67	65.72
2.80	11.59	42.54	48.10	48.66	49.19	51.61	49.99
1.00	7.42	26.68	30.39	31.09	31.90	33.84	33.80
0.50	5.75	20.57	23.49	24.72	25.03	26.52	26.87
0.32	4.86	17.79	20.33	21.28	21.88	23.17	23.55
0.20	3.88	15.14	17.30	18.19	18.81	19.97	20.24
0.13	2.79	12.82	14.67	15.78	16.09	17.33	17.33
0.09	1.31	11.43	13.10	13.95	14.46	15.59	15.49
<i>Specific power consumption</i>							
<i>W</i> (kWh/t)		1.38	1.91	2.03	2.08	2.39	1.98

Table 3
Summary of open circuit tests results performed by manufacturer M2 with porphyritic copper ore.

Test	Feed	M2-P1	M2-P2	M2-P3	M2-P4
<i>Operating conditions</i>					
<i>U</i> (m/s)		0.29	0.29	0.29	0.29
<i>R_p</i> (bar)		30	40	50	40
Size (mm)	Percent passing (%)				
31.50	100.00	100.00	100.00	100.00	100.00
22.40	99.20	100.00	100.00	100.00	100.00
16.00	78.20	97.60	98.10	97.90	97.50
11.20	55.20	87.30	91.50	91.80	90.60
8.00	45.80	80.30	84.00	85.50	81.70
4.00	31.10	64.90	69.10	70.80	67.20
2.00	25.90	53.30	57.40	58.40	55.40
1.00	21.70	44.70	47.90	48.80	47.00
0.50	17.80	37.40	40.80	39.90	39.80
0.25	13.70	29.40	32.90	30.90	31.60
0.20	12.50	26.70	30.00	28.10	28.80
0.09	8.40	17.90	20.80	19.10	20.00
0.05	5.10	11.60	14.00	12.60	13.50
<i>Specific power consumption</i>					
<i>W</i> (kWh/t)		1.00	1.38	1.71	1.57

Table 4
Summary of open circuit tests results performed by manufacturer M2 with andesitic copper ore.

Test	Feed	M2-A1	M2-A2	M2-A3	M2-A4
<i>Operating conditions</i>					
<i>U</i> (m/s)		0.29	0.29	0.29	0.29
<i>R_p</i> (bar)		30	40	50	40
Size (mm)	Percent passing (%)				
31.50	100.00	100.00	100.00	100.00	100.00
22.40	99.20	100.00	100.00	100.00	100.00
16.00	78.20	97.50	97.20	97.00	98.90
11.20	55.20	88.20	89.50	89.80	94.80
8.00	45.80	79.10	81.00	84.00	87.50
4.00	31.10	60.80	65.80	68.20	68.60
2.00	25.90	46.80	51.60	53.60	53.10
1.00	21.70	36.50	40.40	42.30	41.70
0.50	17.80	29.20	32.00	33.10	34.20
0.25	13.70	23.80	25.70	26.40	28.10
0.20	12.50	22.20	24.00	24.40	26.30
0.09	8.40	17.00	18.50	18.40	20.20
0.05	5.10	12.30	13.60	13.30	14.60
<i>Specific power consumption</i>					
<i>W</i> (kWh/t)		1.04	1.47	1.92	2.23

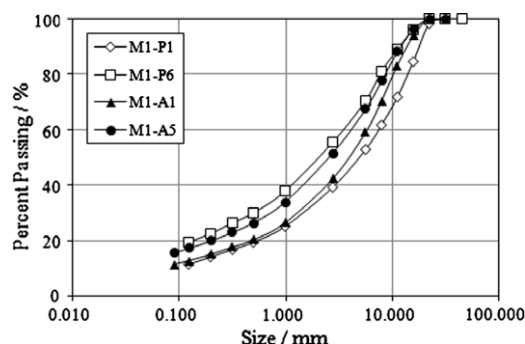


Fig. 5. Experimental product size distributions. Manufacturer M1 and almost the same peripheral velocity, *U*. M1-P1 and M1-P6 (porphyritic ore, *R_p* = 41 and 76 bar, respectively). M1-A1 and M1-A5 (andesitic ore, *R_p* = 39 and 75 bar, respectively).

(marked in the figure) seems to be out of order. Without considering that specific point, the correlation coefficient would be 96%.

For each set of data (Tables 1–4), corresponding to a manufacturer-ore type combination, the parameters of the HPGR

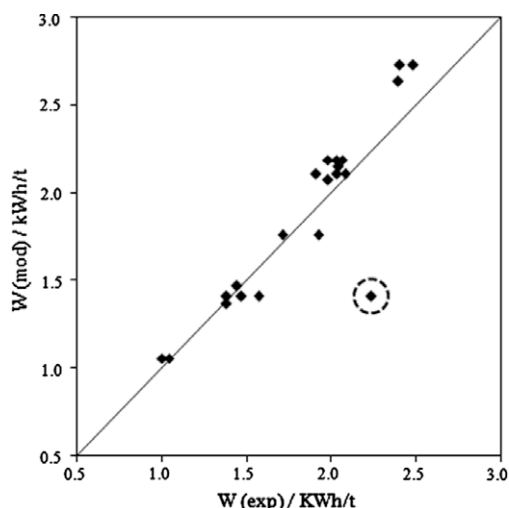


Fig. 6. Validation of the specific energy consumption equation.

particle size distribution model (Eqs. (16), (25), (26), and (27)) were fitted. The experimental data of each set were randomly split in two subsets: one for fitting the model parameters (training set) and the remaining one for validation purposes (validation set). The fitting procedure considered two steps. In the first step, all model parameters were fitted to the data corresponding to each lithology, for both manufacturers simultaneously. In the second

step, the breakage parameters ($\alpha_1, \alpha_2, \alpha_3$) obtained in the previous step were kept constant, while the rest of the model parameters were fitted separately for each manufacturer.

The model parameters were estimated using the gradient descent algorithm to minimize the sum of least squares between the experimental data and the modelled data. As a goodness of fit indicator, the correlation coefficient (R^2) and the chi-square statistic (χ^2) were determined. The results of the model fitting procedure are shown in Table 5.

For a 95% confidence interval and 5 degrees of freedom calculated as: number of size classes – (number of model parameters + 1), the null hypothesis (the modelled and experimental particle size distributions are equal) is accepted if the chi-square statistic is less than 11.1 (Himmelblau, 1970). The results show a good fitting ($R^2 > 98\%$) and ($\chi^2 < 11.1$), however in some of the edge (3) and total (1) distributions the chi-square test fails although the R^2 indicator is greater than 98%.

The model parameters obtained for each ore and manufacturer are shown in Table 6.

4.1. Validation of the particle size distribution model

For validation purposes the remaining subsets of data were compared with simulation results obtained with the model, using as fixed parameters those parameters obtained by the model fitting procedure shown above (Table 6). Table 7 shows the predictive capability indicators comparing the predicted and the experimental data corresponding to the validation subsets.

Table 5
Mean square error and goodness of fit indicators of the training subset.

Test	Mean square error,%			χ^2 statistic			R^2		
	Centre	Edge	Total	Centre	Edge	Total	Centre	Edge	Total
<i>Manufacturer M1, porphyritic ore</i>									
M1-P1	4.53	5.77	2.88	5.57	12.73	3.85	1.00	0.99	1.00
M1-P2	3.77	6.39	3.19	1.27	15.82	11.42	1.00	1.00	1.00
M1-P5	3.64	4.25	2.99	5.58	7.20	3.13	0.99	1.00	1.00
M1-P6	2.42	4.18	1.82	1.28	7.62	1.97	1.00	1.00	1.00
M1-P7	2.62	3.28	2.53	3.13	3.05	2.27	1.00	1.00	1.00
<i>Manufacturer M1, andesitic ore</i>									
M1-A1	2.80	4.44	2.94	3.09	6.85	3.66	1.00	1.00	1.00
M1-A2	2.29	6.16	2.74	2.87	12.06	3.77	1.00	1.00	1.00
M1-A3	2.63	5.79	2.59	5.68	10.16	3.72	1.00	1.00	1.00
M1-A5	2.71	5.23	2.28	4.45	8.86	2.85	1.00	1.00	1.00
<i>Manufacturer M2, porphyritic ore</i>									
M2-P2	3.85	3.72	3.46	8.98	6.96	7.50	1.00	1.00	1.00
M2-P3	4.94	3.44	3.30	8.84	6.17	6.14	1.00	1.00	1.00
<i>Manufacturer M2, andesitic ore</i>									
M2-A1	3.58	3.82	1.74	8.23	4.46	2.07	1.00	1.00	1.00
M2-A3	2.25	3.17	2.15	4.60	4.63	3.64	1.00	1.00	1.00

Table 6
Model parameters for each manufacturer and ore type.

Data set	Model Parameters						
	α_1	α_2	α_3	S_1^E	ζ_1	ζ_2	a
<i>Porphyritic ore</i>							
Manufacturer M1	0.20	0.20	3.51	0.66	-1.26	-0.70	0.22
Manufacturer M2				2.38	0.69	0.03	0.34
<i>Andesitic ore</i>							
Manufacturer M1	0.13	0.15	2.86	1.43	-0.06	-0.46	0.21
Manufacturer M2				3.68	1.28	0.11	0.26
Acceptable variation (%) ^a	7.48	10.01	4.13	3.94	3.98	4.29	21.05

^a Parameter confidence limit. Possible relative variation of each parameter value, causing that the increase in the model fitting error does not exceed 5%.

Table 7
Predictive capability of the particle size distribution model.

Test	Mean square error (%)			χ^2 statistic			R^2		
	Centre	Edge	Total	Centre	Edge	Total	Centre	Edge	Total
<i>Manufacturer M1, porphyritic ore</i>									
M1-P3	2.30	3.86	1.80	1.75	6.34	1.45	1.00	1.00	1.00
M1-P4	2.56	3.79	2.01	2.32	9.37	1.87	1.00	1.00	1.00
<i>Manufacturer M1, andesitic ore</i>									
M1-A4	2.20	6.13	2.31	5.70	10.50	4.02	1.00	1.00	1.00
M1-A6	2.44	4.41	2.12	3.95	10.41	4.03	1.00	1.00	1.00
<i>Manufacturer M2, porphyritic ore</i>									
M2-P1	4.53	5.45	3.91	14.16	21.43	10.64	0.99	1.00	0.99
M2-P4	3.63	3.95	3.17	6.96	8.08	5.87	1.00	0.99	1.00
<i>Manufacturer M2, andesitic ore</i>									
M2-A2	2.49	1.85	1.52	3.05	1.46	1.93	1.00	1.00	1.00
M2-A4	3.23	3.55	2.87	5.11	5.77	6.27	1.00	1.00	1.00

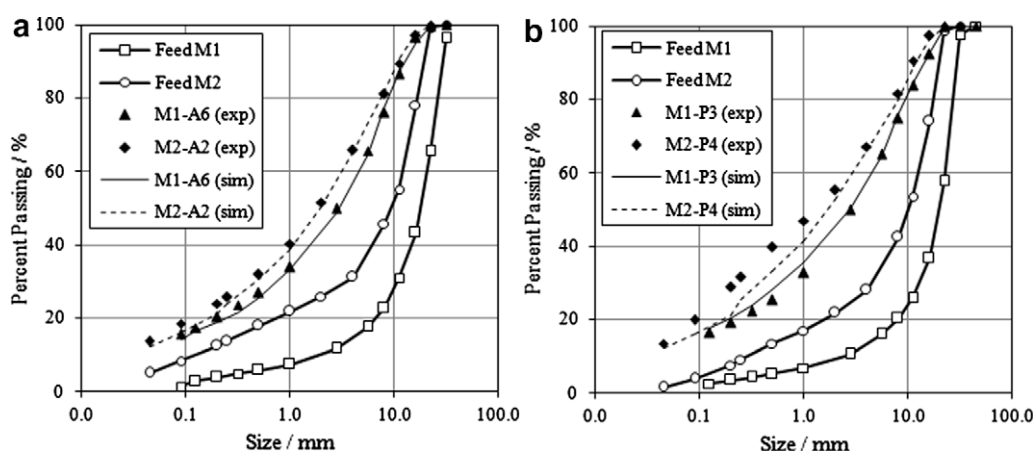


Fig. 7. Experimental and predicted curves of the total product particle size distribution for each manufacturer and each ore type. (a) Andesitic ore and (b) Porphyritic ore.

The prediction quality is good for the particle size distribution of the total products. The correlation coefficient values are all over 98%, but the chi-square test fails in two of the predictions (centre and edge for the same test) of product size distribution.

In Fig. 7 the validation graphs, with the particle size distribution of the total product, for each manufacturer and each ore type are shown.

5. Conclusions

A phenomenological and steady-state model of the HPGR was developed as a function of operating variables, equipment specifications and ore characteristics. A novel approach was used in the estimation of the product size distributions.

The results of the pilot scale tests (Tables 1–4) showed the energy savings of the HPGR, the specific energy consumption was less than 3 kWh/t and the model was quite accurate in this prediction.

The results of the model fitting procedure showed that the parameters of the selection function are manufacturer-dependent. The selection function curves for each manufacturer were very similar, independently of the ore. Between manufacturers M1 and M2, greater differences were observed for coarser sizes, but quite small for the finer ones. With respect to the parameter *a* (edge fraction) the values for manufacturer M1 were quite similar (see Table 6).

The experimental results showed that for different operating pressures, R_p , different product size distributions were obtained (see Fig. 5). It was also evident that the ore type caused a small effect, especially when a higher R_p was used, with a lower R_p

the differences were more evident (see Fig. 5). The differences of grinding between both manufacturers (see Fig. 7) are explained by the differences in the operating pressure R_p . While the manufacturer M1 tests shown in Fig. 7a were performed at higher R_p values (59–60 bar), the manufacturer M2 tests shown in Fig. 7b corresponded to lower R_p values (30–40 bar). These R_p differences explain the different size reduction more than the different manufacturer.

Although the chi-square goodness of fit tests failed in few (4 out of 39) of all particle size distributions, the model fit is good. For the fitting of the total particle size distributions, mean square errors lower than 3.46% with an average of 2.66%, were obtained.

Finally, the predictive capability of the model is accurate, a correlation coefficient R^2 greater than 80% for the prediction of the specific energy consumption (96% if a questionable test is not used). In the prediction of the particle size distributions, the chi-square tests failed in two (out of 24) of the particle size distributions (centre and edge for the same test). For the prediction of the total particle size distributions, mean square errors lower than 3.91% with an average of 2.46%, were obtained.

Appendix A. Simulation example

The following calculations were made for a HPGR of $D = 1.00$ m and $L = 0.75$ m operating at $R_p = 60$ bar. The ore density is $\rho = 2.7$ t/m³ and the bulk density is $\rho_a = 1.6$ t/m³. The operating gap, the roll peripheral velocity and the density of the product at the extrusion zone were calculated by estimations mentioned by Klymowsky et al. (2002): $s_0 = 0.03D$, $U = D$ and $\delta = 0.85\rho$. Then,

$$s_0 = 0.03 \text{ m}$$

$$U = 1.00 \text{ m/s}$$

$$\delta = 2.3 \text{ t/m}^3$$

A.1. Determination of throughput and inter particle compression angle

Step 1: Calculate the inter particle compression angle from Eq. (6):

$$\alpha_{IP} = \arccos \left(\frac{1}{2 \times 1.00} [(0.03 + 1.00) + \sqrt{(0.03 + 1.00)^2 - \frac{4 \times 0.03 \times 2.30 \times 1.00}{1.60}}] \right) = 9.47^\circ$$

Step 2: Calculate the HPGR throughput from Eq. (7):

$$G_s = 3600 \times 2.30 \times 0.03 \times 0.75 \times 1.00 = 186.3 \text{ tph}$$

A.2. Power draw and specific energy consumption calculation

Step 1: Calculate the compression force from Eq. (8)

$$F = 100 \times 60 \times \frac{1.00}{2} \times 0.75 = 2250 \text{ kN}$$

Step 2: Calculate the total power draw from Eq. (10)

$$P = 2 \times 2250 \sin \left(\frac{9.47}{2} \right) \times 1.00 = 371.46 \text{ kW}$$

Step 3: Calculate the specific energy consumption from Eq. (11) as

$$W = \frac{371.46}{186.30} = 1.99 \text{ kWh/t}$$

A.3. Particle size distribution calculation

The calculations were done using the parameters for Andesitic ore and Manufacturer 1 and a given particle size distribution of the feed. For simplification purposes, three blocks ($N_B = 3$) and three size classes were considered.

Size (mm)	Percent passing (%)
50.80	100.00
25.40	50.00
12.70	25.00

Step 1: Calculate the breakage and specific selection matrices from Eqs. (18)–(20).

$$b_{ij} = \begin{pmatrix} 0.00 & 0.00 & 0.00 \\ 0.76 & 0.00 & 0.00 \\ 0.24 & 1.00 & 0.00 \end{pmatrix}, \quad S_i^E = \begin{pmatrix} 1.43 & 0.00 & 0.00 \\ 0.00 & 1.19 & 0.00 \\ 0.00 & 0.00 & 0.40 \end{pmatrix}$$

Step 2: Calculate the height of the particle bed compression zone from Eq. (15).

$$z^* = \frac{1.00}{2} \sin(9.47) = 0.08 \text{ m}$$

Step 3: Calculate the critical size from Eq. (12)

$$x_c = 0.03 + 1.00(1 - \cos(9.47)) = 0.04 \text{ m} = 40 \text{ mm}$$

The class sizes considered in the feed are lower than the critical size, from Fig. 3 all the ore was crushed by particle bed compression.

Step 4: Calculate the holdup of each block using Eq. (22)

$$H_k = \frac{1}{3} \times 186.30 \times \frac{0.08}{3600 \times 1.00} = 1.38 \times 10^{-3} \text{ t}$$

Step 5: Calculate the centre and the power of each block using Eqs. (24) and (23)

$$y_1 = \frac{0.75}{2 \times 3} (2 \times 1 - 3 - 1) = -0.25, \quad y_2 = 0, \quad y_3 = 0.25$$

$$P_1 = 371.46 \times \frac{(0.75^2 - 4 \times 0.25^2)}{(0.75^2 - 4 \times 0.25^2) + (0.75^2 - 4 \times 0.00^2) + (0.75^2 - 4 \times 0.25^2)} = 96.58 \text{ kW}$$

$$P_2 = 174.59 \text{ kW}$$

$$P_3 = 96.58 \text{ kW}$$

Step 6: Calculate the rate of breakage of each block using Eq. (21)

$$S_{1,1} = \frac{96.58}{1.38 \times 10^{-3}} 1.43 = 100079.28, \quad 1/h = 27.80 \text{ 1/s},$$

$$S_{2,1} = 23.13 \text{ 1/s}, \quad S_{3,1} = 7.78 \text{ 1/s}$$

$$S_{2,1} = 50.25 \text{ 1/s}, \quad S_{2,2} = 41.82 \text{ 1/s}, \quad S_{2,3} = 14.06 \text{ 1/s}$$

$$S_{3,1} = 27.80 \text{ 1/s}, \quad S_{3,2} = 23.13 \text{ 1/s}, \quad S_{3,3} = 7.78 \text{ 1/s}$$

Step 7: Calculate the particle size distribution of each size class and block using Eq. (16)

$$p_{1,1} = p_{1,3} = 50 \exp \left(-\frac{27.80}{1.00} 0.08 \right) = 5.41$$

$$p_{2,1} = p_{2,3} = \frac{0.76 \times 27.80}{23.13 - 27.80} 50 \exp \left(-\frac{27.80}{1.00} 0.08 \right) + \left(50 - \frac{0.76 \times 27.80}{23.13 - 27.80} 50 \right) \exp \left(-\frac{23.13}{1.00} 0.08 \right) = 18.94$$

$$p_{3,1} = p_{3,3} = 100 - p_{2,1} - p_{1,1} = 75.65$$

$$p_{1,2} = 0.90$$

$$p_{2,2} = 9.34$$

$$p_{1,3} = 90.57$$

Step 8: Calculate the total particle size distribution from Eq. (26)

$$p_1^{\text{HPGR}} = \frac{1}{3} (5.41 + 0.90 + 5.41) = 3.91$$

$$p_2^{\text{HPGR}} = 15.74$$

$$p_3^{\text{HPGR}} = 80.31$$

Step 9: Calculate the edge particle size distribution from Eq. (25)

$$E = 0.50 \times 0.21 \times 3.00 = 0.32 (0.5a N_B)$$

$$p_1^E = \frac{1}{0.32} [0.32 \times 5.41] = 5.41$$

$$p_2^E = 18.94$$

$$p_3^E = 75.65$$

Step 10: Calculate the centre particle size distribution from Eq. (27)

$$p_1^C = \frac{1}{1 - 0.21} (3.91 - 0.21 \times 5.41) = 3.51$$

$$p_2^C = 14.89$$

$$p_3^C = 81.60$$

References

- Austin, L.G., 1997. Mill power for high-pressure grinding rolls in coal grinding. Minerals and Metallurgical Processing 14 (3), 18–26.

- Austin, L.G., Luckie, P.T., 1972. Estimation of non-normalized breakage distribution parameters from batch grinding. *Powder Technology* 5 (5), 267–277.
- Bearman, R., 2006. High-pressure grinding rolls – characterizing and defining process performance for engineers. In: Kawatra, S. (Ed.), *Advances in Comminution*. SME Inc., Littleton, pp. 3–14.
- Daniel, M.J., Morrell, S., 2004. HPGR model verification and scale-up. *Minerals Engineering* 17 (11–12), 1149–1161.
- Danilkewich, H., Hunter, I., 2006. HPGR challenges and growth opportunities. In: Allan, M.J., Major, K., Flintoff, B.C., Klein, B., Mular, A.L. (Eds.), *Proc. International Conference on Autogenous and Semiautogenous Grinding Technology 2006*, vol. IV. Department of Mining Engineering, University of British Columbia, Vancouver, B.C., pp. 27–44.
- Herbst, J.A., Fuerstenau, D.W., 1980. Scale-up procedure for continuous grinding mill design using population balance models. *International Journal of Mineral Processing* 7, 1–31.
- Himmelblau, D.M., 1970. *Process Analysis by Statistical Methods*, first ed. Sterling Swift, Texas.
- Klymowsky, R., Patzelt, N., Knecht, J., Burchardt, E., 2002. Selection and sizing of high pressure grinding rolls. In: Mular, A., Halbe, D., Barratt, D. (Eds.), *Proc. Mineral processing plant design, practice and control*, vol. 1. SME Inc., Littleton, pp. 636–668.
- Klymowsky, R., Patzelt, N., Knecht, J., Burchardt, E., 2006. An overview of HPGR technology. In: Allan, M.J., Major, K., Flintoff, B.C., Klein, B., Mular, A.L. (Eds.), *Proc. International Conference on Autogenous and Semiautogenous Grinding Technology 2006*, vol. IV. Department of Mining Engineering, University of British Columbia, Vancouver, B.C., pp. 11–26.
- Lim, W.I.L., Campbell, J.J., Tondo, L.A., 1997. The effect of rolls speed and rolls surface pattern on high pressure grinding rolls performance. *Minerals Engineering* 10 (4), 401–419.
- Lubjuhn, U., 1992. Axiale Druckverteilung. <www.yellow-bridge.de/Gbw/druck_axial.htm>.
- Morley, C., 2006. High-pressure grinding rolls – a technology review. In: Kawatra, S. (Ed.), *Advances in Comminution*. SME Inc., Littleton, pp. 15–39.
- Morrell, S., Shi, F., Tondo, L.A., 1997. Modelling and scale-up of high pressure grinding rolls. In: *Proc. XX International Mineral Processing Congress. IMPC*, Aachen, Germany.
- Oestreicher, C., Spollen, C.F., 2006. HPGR versus SAG mill selection for the Los Bronces grinding circuit expansion. In: Allan, M.J., Major, K., Flintoff, B.C., Klein, B., Mular, A.L. (Eds.), *Proc. International Conference on Autogenous and Semiautogenous Grinding Technology 2006*, vol. IV. Department of Mining Engineering, University of British Columbia, Vancouver, B.C., 2006, pp. 110–123.
- Patzelt, N., Klymowsky, R., Knecht, J., Burchardt, E., 2006. High-pressure grinding rolls for gold/copper applications. In: Kawatra, S. (Ed.), *Advances in Comminution*. SME Inc., Littleton, pp. 51–67.
- Reid, K.J., 1965. A solution to the batch grinding equation. *Chemical Engineering Science* 20 (11), 953–963.
- van Drunick, W., Smit, I., 2006. Energy efficient comminution – HPGR experience at Anglo research. In: Allan, M.J., Major, K., Flintoff, B.C., Klein, B., Mular, A.L. (Eds.), *Proc. International Conference on Autogenous and Semiautogenous Grinding Technology 2006*, vol. IV. Department of Mining Engineering, University of British Columbia, Vancouver, B.C., pp. 124–139.